Redshift drift in axially symmetric quasispherical Szekeres models

Priti Mishra[*]

Department of Astronomy and Astrophysics, Tata Institute of Fundamental Research, Homi Bhabha Road,
Colaba, Mumbai, 400005 Maharashtra, India

Marie-Noëlle Célérier[†]

Laboratoire Univers et Théories (LUTH), Observatoire de Paris, CNRS, Université Paris-Diderot 5 place Jules Janssen,
92190 Meudon, France

Tejinder P. Singh[‡]

Department of Astronomy and Astrophysics, Tata Institute of Fundamental Research, Homi Bhabha Road,
Colaba, Mumbai, 400005 Maharashtra, India

Models of inhomogeneous universes constructed with exact solutions of Einstein's general relativity have been proposed in the literature with the aim of reproducing the cosmological data without any need for a dark energy component. Besides large scale inhomogeneity models spherically symmetric around the observer, Swiss-cheese models have also been studied. Among them, Swiss cheeses where the inhomogeneous patches are modeled by different particular Szekeres solutions have been used for reproducing the apparent dimming of the type Ia supernovae. However, the problem of fitting such models to the type Ia supernovae data is completely degenerate and we need other constraints to fully characterize them. One of the tests which is known to be able to discriminate between different cosmological models is the redshift drift. This drift has already been calculated by different authors for Lemaître-Tolman-Bondi models. We compute it here for one particular axially symmetric quasispherical Szekeres Swiss cheese which has previously been shown to reproduce to a good accuracy the type Ia supernovae data, and we compare the results to the drift in the ΛCDM model and in some Lemaître-Tolman-Bondi models that can be found in the literature. We show that it is a good discriminator between them. Then, we discuss our model's remaining degrees of freedom and propose a recipe to fully constrain them.

I. INTRODUCTION

The last two decades have witnessed a phenomenal increase of the available cosmological data. Analyzed in the framework of a Friedmann-Lemaître-Robertson-Walker (FLRW) homogeneous cosmology, they have yielded the concordance model where more than 95% of the Universe content is of unknown nature. Among these 95%, around 75% of the Universe energy density is ascribed to the influence of some rather exotic component called dark energy. But dark energy has never been directly observed either in the Universe or in laboratories, and it has very exotic properties; namely, it is a kind of fluid with negative pressure or a cosmological constant with an amplitude too small to account for the vacuum energy in the current standard model of particle physics. This has led some authors to study whether the observations could not be given a more natural explanation in the framework of inhomogeneous models constructed with exact solutions of Einstein's field equations without any dark energy component.

The models most often found in the literature are roughly of two kinds: one patch large scale inhomogeneous Lemaître-Tolman-Bondi (LTB) models, spherically symmetric around the observer [1–17], and Swiss-cheese models in which the patches can be either spherically symmetric LTB holes [18–24] or nonspherical Szekeres patches [25,26].

Since the LTB solutions are determined by two free functions of the radial coordinate plus a radial coordinate choice, two independent sets of data are necessary and sufficient to define them, e.g., angular distance and galaxy number counts [14,27–30]. In the most recent works devoted to solve the dark energy problem with zero-Λ LTB models, such solutions have been constrained by two or more sets of data measured on our past light cone [3,7–9,12,13,15–17,31–33]. By construction, we are thus left with a degeneracy as regards the ΛCDM model, because in both cases, homogeneous and inhomogeneous cosmology, the same data are reproduced without the possibility to discriminate between the models. However, it has been suggested that this degeneracy can only occur if the LTB model is not smooth at the center; otherwise, the models are distinguishable [34,35].

The degeneracy is even worse, when a few independent data sets are used, for models constructed with Szekeres

[*]priti@tifr.res.in
[†]marie-noelle.celerier@obspm.fr
[‡]tpsingh@tifr.res.in

solutions which are determined by five free functions of the radial coordinate plus a radial coordinate choice in the most general case. Even if this number can be reduced to three in the case of axial symmetry, as we discuss in Sec. V, the mere supernova data used to constrain the models in Ref. [25] is far from being sufficient for fully determining them.

This is the reason why tests using the redshift drift have been recently proposed to deal with this issue. The redshift drift is the temporal variation of the redshift of distant sources when the observation of the same source is done at observer's different proper times in an expanding universe. It allows one to make observations on the past light cones of an observer at different cosmological times, therefore giving access to a slice of space-time. It is thus a good discriminator between different cosmological models able to reproduce the observational data on our current past light cone. This effect has first been considered by Sandage [36] and then by McVittie [37]. In FLRW models, when the Universe expansion decelerates, all redshifts decrease with time. In FLRW models where the expansion is recently accelerating, like in the ΛCDM model, sources with redshifts $\lesssim 2.5$ exhibit a positive redshift drift. In Ref. [38], this effect has been proposed to test the "Copernican principle" and to close the reconstruction problem of an LTB model from the luminosity distance as inferred from the supernova data. Other authors have since examined this effect for one patch zero-Λ LTB models [39,40]. It has been shown in Ref. [41] that this effect is the only currently proposed one able to test, in principle, the LTB one patch models against the ΛCDM model "outside the past light cone," provided spherical symmetry is but a mathematical simplification and one considers LTB models as exhibiting an energy density smoothed out over angles around us. However, other proposals designed to test specific LTB models considered as a single exact space-time and relying on conditions inside the observer's light cone can be found in the literature, e.g., tests using the baryon acoustic oscillation scale [16,31], the kinematic Sunyaev-Zel'dovich effect [8,32,33] or the Compton y distortion of the cosmic microwave background spectrum [16,42].

Here, we want to study the redshift drift in Swiss-cheese models which seem to represent more closely our observed Universe with its voids and filamentary patterns.

For voids, the spherically symmetric shape of the holes can be considered as a good approximation since non-spherical voids evolve towards a spherical configuration. Actually, it has been shown, using the top-hat void model, that the smaller axis of an underdense ellipsoid stretches out faster than the longer one implying that voids become increasingly spherical as they evolve [43]. Conversely, overdense ellipsoids tend to form pancakes and filamentary structures which are what we observe in the Universe. This is the reason why we choose to study a Swiss cheese with nonspherically symmetric overdense patches.

An inhomogeneous exact solution of general relativity with no symmetry at all (no Killing vector) is the Szekeres model [44]. Among its subclasses, the quasispherical Szekeres (QSS) case is best suited for our purpose since it possesses all three FLRW classes of models as an homogeneous limit and can therefore be matched to any kind of FLRW background. However, it has been shown in Refs. [45,46] that, in a general Szekeres model, generic light rays do not have repeatable paths (RLPs); i.e., two rays sent from the same source at different times to the same observer do not proceed through the same succession of intermediate matter particles, implying thus an angular drift of the source on the sky. This implies that, in such models, the light rays emitted from a source at different time coordinates are emitted in different directions and therefore reach different loci at the border of each patch. Since we integrate the null geodesic and redshift-drift equations for a sequence of such different time coordinates for each source, i.e., for each redshift z, this makes impossible the choice of the locus of the matching between two patches and thus impairs the construction of Swiss-cheese models. There are only two Szekeres classes, besides FLRW models, where RLPs exist, the most interesting for our purpose being the axially symmetric Szekeres models, in which the RLPs are the null geodesics intersecting every space of constant time on the axis of symmetry.

Actually, such a class of models have been used in Ref. [25] (hereafter BC) to construct QSS Swiss cheeses which can reproduce the supernova data. The model which we consider here is BC's model 5 which best reproduces these data and which is a model with overdense patches matched to an open FLRW background. In this model, the observer is located at the origin of the first patch and the sources, at redshifts ranging from $z = 0$ to $z \sim 2.5$, can be anywhere on null geodesics axially directed towards the observer. Of course, this Swiss-cheese model must be still considered as a very simplified toy model since axial symmetry is not a generic property of structures in the observed Universe.

Anyhow, it is important to compute the redshift drift in such configurations and to compare it to the results in the ΛCDM model and other LTB models.

Inhomogeneous exact models have been sometimes criticized on the ground that they exhibit more degrees of freedom than FLRW models and are thus able to fit more easily the data. Another interesting question to be addressed is therefore: how many independent data sets do we need to fully reconstruct an axially symmetric QSS model?

It has already been shown in Ref. [38] that the combination of luminosity distance and redshift-drift data allows one to fully constrain a spherically symmetric space-time. This applies, in particular, to LTB models. It has also been shown in Ref. [29] that, for any given isotropic observations of the apparent luminosity $l(z)$ and of the galaxy

number count $n(z)$, with any given source evolution functions $\hat{L}(z)$ and $\hat{m}(z)$, a set of functions determining a zero-Λ LTB model can be found to make the LTB observational relations fit the observations.

We demonstrate here, as a first step towards a more general theorem to be applied to QSS models without any symmetry, that an axially symmetric zero-Λ Szekeres model needs three independent observation sets to be fully reconstructed.

The structure of the present paper is as follows. In Sec. II, we present the Szekeres models and the particular QSS subclass used in this paper. Section III is devoted to the derivation of the differential equation giving the redshift drift. In Sec. IV, we display our result for the computation of the drift in BC model 5 and we compare it to that of the ΛCDM model and other LTB models studied in the literature. In Sec. V, we discuss the issue of closing the reconstruction of our type of model with a sufficient number of data sets, and we propose a solution for axially symmetric QSS models. In Sec. VI, we present our conclusions.

II. SZEKERES MODELS

The Szekeres solutions [44] are the most general solutions of Einstein's equations one can obtain with a dust gravitational source. They have no symmetry, i.e., no Killing vector, and are therefore well suited to describe a lumpy universe. Their metric in comoving coordinates and synchronous time gauge is

$$d s^2 = c^2 dt^2 - e^{2\alpha} dr^2 - e^{2\beta}(dx^2 + dy^2), \quad (2.1)$$

where α and β are functions of (t, r, x, y) to be determined by the field equations.

There are two families of Szekeres solutions. The class II family, where $\beta' = 0$ (here the prime denotes derivative with respect to r), is a simultaneous generalization of the Friedmann and Kantowski-Sachs models. Its spherically symmetric limit is the Datt-Ruban solution whose physical interpretation is not clear [47,48]. The class I family of solutions is obtained when $\beta' \neq 0$. They contain the LTB solution as a spherically symmetric limit. We choose therefore this class of solutions to study the redshift drift in Szekeres models. After solving the Einstein equations, its metric can be written, after a change of parametrization more convenient for our purpose [49],

$$d s^2 = c^2 dt^2 - \frac{(\Phi' - \Phi E'/E)^2}{\epsilon - k} dr^2 - \Phi^2 \frac{(dx^2 + dy^2)}{E^2},$$
$$(2.2)$$

where $\epsilon = 0, \pm 1$, Φ is a function of t and r, k is a function of r, and

$$E = \frac{S}{2}\left[\left(\frac{x - P}{S}\right)^2 + \left(\frac{y - Q}{S}\right)^2 + \epsilon\right], \quad (2.3)$$

with $S(r)$, $P(r)$, and $Q(r)$ functions of r.

A. Quasispherical Szekeres models

As it appears from (2.2), only $\epsilon = +1$ allows the solution to have the three Friedmann limits (hyperbolic, flat and spherical). This is induced by the requirement of a Lorentzian signature for the metric. Since we are interested in the Friedmann limit of our model which we expect to become homogeneous at very large scales, i.e., that of the last scattering, we focus only on the $\epsilon = +1$ case. It is called the QSS model.

Its metric, obtained with $\epsilon = +1$ in Eq. (2.2), becomes

$$d s^2 = c^2 dt^2 - \frac{(\Phi' - \Phi E'/E)^2}{1 - k} dr^2 - \Phi^2 \frac{(dx^2 + dy^2)}{E^2},$$
$$(2.4)$$

where

$$E = \frac{S}{2}\left[\left(\frac{x - P}{S}\right)^2 + \left(\frac{y - Q}{S}\right)^2 + 1\right]. \quad (2.5)$$

Applying the Einstein equations to the metric (2.4) and assuming the energy momentum tensor is that of dust, the Einstein equations reduce to the following two:

$$\frac{1}{c^2}\dot{\Phi}^2 = \frac{2M}{\Phi} - k + \frac{1}{3}\Lambda\Phi^2, \quad (2.6)$$

where the dot denotes derivation with respect to t, Λ is the cosmological constant and $M(r)$ is an arbitrary function of r related to the density ρ via

$$\kappa\rho c^2 = \frac{2M' - 6ME'/E}{\Phi^2(\Phi' - \Phi E'/E)}, \quad (2.7)$$

where $\kappa = 8\pi G/c^4$.

The 3D Ricci scalar is

$$3\mathcal{R} = 2\frac{k}{\Phi^2}\left(\frac{\Phi k'/k - 2\Phi E'/E}{\Phi' - \Phi E'/E} + 1\right). \quad (2.8)$$

The Weyl curvature tensor decomposed into its electric and magnetic parts is

$$E^\alpha{}_\beta = C^\alpha{}_{\gamma\beta\delta}u^\gamma u^\delta$$
$$= \frac{M(3\Phi' - \Phi M'/M)}{3\Phi^3(\Phi' - \Phi E'/E)}\text{diag}(0, 2, -1, -1), \quad (2.9)$$

$$H_{\alpha\beta} = \frac{1}{2}\sqrt{-g}\epsilon_{\alpha\gamma\mu\nu}C^{\mu\nu}{}_{\beta\delta}u^\gamma u^\delta = 0,$$

where $\epsilon_{\alpha\gamma\mu\nu}$ is the four-dimensional Levi-Cività symbol. It can be easily noticed that (2.6), (2.7), (2.8), and (2.9) reduces to the LTB equations once E'/E is set to vanish.

Since (2.6) is the same in this model as in the LTB model, the bang time function $t_B(r)$ follows from (2.6) in the same manner as

$$\int_0^\Phi \frac{d\tilde{\Phi}}{\sqrt{-k + 2M/\tilde{\Phi} + \frac{1}{3}\Lambda\tilde{\Phi}^2}} = c[t - t_B(r)]. \quad (2.10)$$

All the formulas given so far being covariant under coordinate transformations of the form $\tilde{r} = g(r)$, this means that one of the functions $k(r)$, $S(r)$, $P(r)$, $Q(r)$, $M(r)$ and $t_B(r)$ can be fixed at our convenience by the choice of g. Hence, each Szekeres solution is fully determined by only five functions of r. In the following, we choose S, P, Q, M and t_B, and we make the coordinate choice: $\Phi(t_0, r) = r$.

B. Axially symmetric QSS models. Null cone equations

We have seen in Sec. I that only axially symmetric QSS models possess RLPs and are therefore more suited for an easy study of the redshift drift in Swiss-cheese models. Moreover, in these models, the only RLPs are axially directed null geodesics. Since, in our Swiss-cheese models, we use only radially directed light rays, this implies, as shown in Ref. [50] (see also Ref. [51]), that the Szekeres model should be axially symmetric and that, accordingly, the rays we consider for the computation of the drift are RLPs. The simplest axially symmetric Szekeres model obeys

$$P(r) = x_0 = \text{const}, \qquad Q(r) = y_0 = \text{const}.$$

In this case, the dipole axis is along $x = x_0$ and $y = y_0$ (or in spherical coordinates along the directions $\vartheta = 0$ and $\vartheta = -\pi$).

For the axially directed geodesics ($dx = dy = 0$), we obtain from the null condition in (2.4)

$$\frac{dt}{dr} = \pm \frac{1}{c} \frac{\Phi' - \Phi E'/E}{\sqrt{1 - k}}. \quad (2.11)$$

The plus sign is for $r_e < r_o$ and the minus sign for $r_e > r_o$, with r_e the radial coordinate of the source and r_o the radial coordinate of the observer. Since we put the observer at the origin $r_o = 0$, we use the minus sign in (2.11).

The redshift relation in this case is [51]

$$\ln(1 + z) = -\frac{1}{c} \int_{r_e}^{r_o} dr \frac{\dot{\Phi}' - \dot{\Phi}E'/E}{\sqrt{1 - k}}, \quad (2.12)$$

or equivalently,

$$\frac{dr}{dz} = \frac{c}{1 + z} \frac{\sqrt{1 - k}}{\dot{\Phi}' - \dot{\Phi}E'/E},$$
$$\frac{dt}{dz} = -\frac{1}{1 + z} \frac{\Phi' - \Phi E'/E}{\dot{\Phi}' - \dot{\Phi}E'/E}. \quad (2.13)$$

III. THE REDSHIFT-DRIFT EQUATION FOR AN AXIALLY SYMMETRIC QSS MODEL

The redshift drift is the redshift increase or decrease a comoving observer looking at the same comoving source

on her past light cone can measure while her proper time elapses. That means that the redshift of the source is measured on the observer's two different past light cones.

An equation giving the redshift drift in LTB models was derived in Ref. [40]. We adapt here the reasoning to obtain such an equation for the axially symmetric QSS model.

We consider an observer O located at the origin, with coordinates $(t_0, r = 0)$ (Fig. 1). After an elapsed time δt_0, this comoving observer is at O' $(t_0 + \delta t_0, r = 0)$. A comoving source, with radial coordinate r has, on the past light cone issued from O, redshift $z(r)$ and time coordinate $t(r)$. The same comoving source has, on the light cone issued from O', redshift

$$Z(r) = z(r) + \delta z(r) \quad (3.1)$$

and time coordinate

$$T(r) = t(r) + \delta t(r), \quad (3.2)$$

with $t(r = 0) = t_0$, $z(r = 0) = Z(r = 0) = 0$, $\delta z(r = 0) = 0$ and $\delta t(r = 0) = \delta t_0$.

From the geodesic equations (2.13), the equation for the redshift is

$$\frac{dz}{dr} = \frac{1 + z}{c} \frac{\dot{\Phi}' - \dot{\Phi}E'/E}{\sqrt{1 - k}}. \quad (3.3)$$

Equation (3.1) can be written

$$\frac{d\delta z(r)}{dr} = \frac{dZ(r)}{dr} - \frac{dz(r)}{dr}. \quad (3.4)$$

Inserting (3.3) in (3.4) and considering $\delta z(r)$ and $\delta t(r)$ as negligible with respect to z and t, we keep only the first-order terms in δz and δt and obtain

$$\frac{d\delta z}{dr} = \frac{1 + z}{c} \frac{[\ddot{\Phi}'(t, r) - \ddot{\Phi}(t, r)E'/E]}{\sqrt{1 - k}} \delta t$$
$$+ \frac{\dot{\Phi}'(t, r) - \dot{\Phi}(t, r)E'/E}{\sqrt{1 - k}} \frac{\delta z}{c}. \quad (3.5)$$
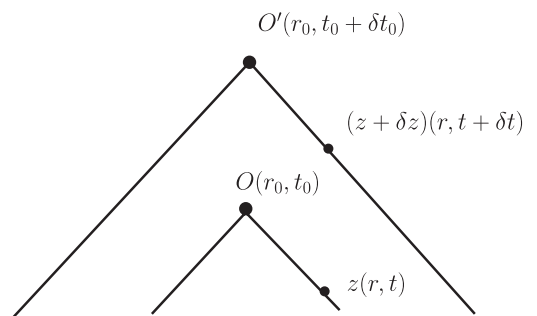
FIG. 1. The redshift drift δz of a source, initially at a redshift z on the past light cone of an observer at O, as measured by the same observer at O' after an elapsed time δt_0 of the observer's proper time.

Now, (3.2) can be written

$$\frac{d\delta t(r)}{dr} = \frac{dT(r)}{dr} - \frac{dt(r)}{dr}. \quad (3.6)$$

Inserting (2.11) with the minus sign in (3.6) and considering $\delta t(r)$ as negligible with respect to t, therefore keeping only the first-order term in δt, we obtain

$$\frac{d\delta t(r)}{dr} = -\frac{1}{c}\frac{\dot{\Phi}'(t,r) - \dot{\Phi}(t,r)E'/E}{\sqrt{1-k}}\delta t. \quad (3.7)$$

We consider the case where the redshift z is monotonically increasing with r and we replace the independent variable r by z. By using

$$\frac{d}{dr} = \frac{dz}{dr}\frac{d}{dz} = \frac{1+z}{c}\frac{\dot{\Phi}' - \dot{\Phi}E'/E}{\sqrt{1-k}}\frac{d}{dz} \quad (3.8)$$

in (3.6) and after some rearrangement, we obtain

$$\frac{d\delta z}{dz} = \frac{\ddot{\Phi}' - \ddot{\Phi}E'/E}{\dot{\Phi}' - \dot{\Phi}E'/E}\delta t + \frac{\delta z}{1+z}. \quad (3.9)$$

Now, we insert (3.8) into (3.7), that gives

$$\frac{d\delta t}{dz} = -\frac{\delta t}{1+z}, \quad (3.10)$$

which we integrate from the observer O at $(t_0, z = 0)$ to the source at (t, z) to obtain

$$\delta t = \frac{\delta t_0}{1+z}. \quad (3.11)$$

We insert this expression for δt into (3.9) and obtain the equation for the redshift drift,

$$\frac{d}{dz}\left(\frac{\delta z}{1+z}\right) = \frac{1}{(1+z)^2}\frac{\ddot{\Phi}' - \ddot{\Phi}E'/E}{\dot{\Phi}' - \dot{\Phi}E'/E}\delta t_0. \quad (3.12)$$

Once δz is obtained by numerically integrating (3.12) for a fixed value of δt_0, the redshift drift follows from its definition $\dot{z} = \delta z/\delta t_0$.

IV. COMPUTATION OF THE REDSHIFT DRIFT IN BC'S SWISS-CHEESE MODEL 5

A. The Swiss-cheese model

As seen above, in the case of axially directed geodesics the equations which describe light propagation and redshift drift simplify significantly. Moreover, density fluctuations (2.7) and curvature fluctuations (2.8) and (2.9) are the largest along the axial axis. When a light ray passes through the origin $E'/E \rightarrow -E'/E$ [51,52]. Since, in the above equations, E'/E is always multiplied by Φ or $\dot{\Phi}$ which are zero at the origin, there is no discontinuity here. Now, a much smaller discontinuity in E'/E (which probably appears due to the imperfect matching in the BC Swiss-cheese model and would probably not occur for a model with perfect matching), of order 4×10^{-6} Mpc^{-1}

(to be compared with the larger discontinuity of order 10^{-3} Mpc^{-1} at the origin) occurs also at the boundaries. However, its magnitude is not sufficient to impact noticeably the results for the redshift drift as can be seen in Fig. 5.

When constructing a Swiss-cheese model, one needs to satisfy the junction conditions at the patch borders. In our models the Szekeres inhomogeneities (the patches) are matched to the Friedmann background (the cheese). These Szekeres patches are arranged so that their boundaries touch wherever a light ray exits its neighbor. Thus the ray immediately enters another patch and spends no time in the Friedmann background. The matching conditions across a comoving spherical surface, $r = $ constant, are the following: the mass inside the junction surface in the Szekeres patch is equal to the mass that would be inside that surface in the homogeneous background (this mass is defined as the mass energy density ρ integrated over the spatial volume inside the junction surface at a fixed time coordinate t); the spatial curvature at the junction surface is the same in both the Szekeres and Friedmann regions, which implies $k_{SZ} = k_F r^2$ and $(k_{SZ})' = 2k_F r$; the bang time and Λ must be continuous across the junction. In our model, $\Lambda = 0$ in both the patches and the cheese.

Besides matching the inhomogeneous patches, one also needs to take care of the null geodesics. However, since we only consider here axial geodesics, the junction is trivial and requires only matching the radial, or equivalently, the time component [53].

The Swiss-cheese model we consider exhibits patches that are described by the following functions:

$$M = \frac{\rho_b \kappa c^2}{2}\int_0^r d\tilde{r}\tilde{r}^2\left[1 + \delta_\rho - \delta_\rho \exp\left(-\frac{\tilde{r}^2}{\sigma^2}\right)\right], \quad (4.1)$$

where $\rho_b = \Omega_m\frac{3H_0^2}{8\pi G}$, $\Omega_m = 0.3$, $H_0 = 68$ km s^{-1} Mpc^{-2}, $\delta_\rho = 0.6$ and $\sigma = 180$ Mpc, $t_B = P = Q = 0$ and $S = (10^3 + \ell)^{\pm 0.8}$, with $\ell = r/$kpc and where $-$ is for propagation from the origin with $E'/E = S'/S = -0.8/(10^3 + \ell)$ and $+$ towards the origin with $E'/E = S'/S = 0.8/(10^3 + \ell)$.

As can be shown from (2.7), (2.8), and (2.9), for $r > 400$ Mpc this model becomes almost homogeneous. We join inhomogeneous patches at $r = 400$ Mpc. By construction, this is not a perfect matching. Only the functions M and k are continuous along this boundary but not for example the curvature [Eqs. (2.8) and (2.9)]. In BC's paper, this nonperfect matching is investigated with the use of a so-called minimum void scenario which exhibits the same arbitrary functions as model 5 but with only one inhomogeneous patch, and therefore no matching. The result is that the χ^2's for reproducing the type Ia supernovae (SNIa) data are exactly the same in both models, the Swiss-cheese model 5 and minimal void model 5, and are equal to 269 for 307 measurements. This shows that the nonperfect matching has no impact at all on SNIa data fitting. Our result for the redshift drift, displayed in Fig. 5, shows that

this nonperfect matching does not impair significantly the calculation of this effect (no visible discontinuities of the derivative at the boundaries there). This ensures the validity of our model for the computation of the redshift drift.

We place the observer at the origin $r = 0$ of the first patch and we consider the light emitted by the sources in the first patch and directed towards the observer. As we have seen above, in this case E'/E is positive. After calculating the redshift drift for all the comoving sources with $0 < r < 400$ Mpc, we are led to the second patch and consider the sources located between the border of this patch and its own origin. The light traveling towards the observer moves away from this origin and we have therefore to change the sign of E'/E. The same occurs when we are led to the other side of the second patch origin. Light emitted from there travels again towards an origin and the sign of E'/E needs once again to be inverted, and so on.

B. The algorithm

In order to calculate the redshift drift, we proceed in the following manner:

(1) To find $k(r)$ we proceed as follows:

After substituting $t = t_0$ and $t_B(r) = 0$ into (2.10) we fix a value of r, which is the upper limit of the integral, between 0 and 400 Mpc. We want such a k which satisfies (2.10). We find that to have a real value of the integrand over the whole range of integration $k < 2M/r$ is necessary. But in the range $0 < k < 2M/r$, we do not obtain any root of (2.10). Therefore we choose the case $k(r) < 0$ for which the parametric solution is the same as in the LTB model and is given by

$$\Phi(r, t) = \frac{M}{(-k)}(\cosh\eta - 1) \qquad (4.2)$$

and

$$t - t_B(r) = \frac{M}{(-k)^{3/2}}(\sinh\eta - \eta), \qquad (4.3)$$

where $\eta(t, r)$ is the parameter.

(2) Using the initial condition $\Phi(t_0, r) = r$ in (4.2) and substituting $\eta = \eta_0$ at $t = t_0$, we get $k(r)$ as

$$-k(r) = \frac{M(r)(\cosh\eta_0 - 1)}{r}. \qquad (4.4)$$

(3) We obtain η_0 by solving numerically (4.3) for $t = t_0$. The numerical value of t_0 for our model is 11.63 Gyr.

(4) Then we find $t(r)$ on the past light cone by numerically solving the null condition equation (2.11) for incoming geodesics. The sign of E'/E is chosen as positive (negative) depending on whether a light ray is moving towards (away from) the origin in the patch in which it is.

(5) Substituting $t(r)$ in (4.3) we obtain $\eta(r)$ on the past light cone issued from O, using which in (4.2) we calculate $\Phi(t(r), r)$ and its derivatives on the past light cone.

(6) Then we numerically solve the first of the two equations (2.13) for the redshift $z(t(r), r)$.

(7) After having found z, we find the redshift drift at this z by numerically solving (3.12).

The various functions obtained by this procedure are described in the next subsection.

C. The results

The results obtained by the numerical computation described above are plotted in Figs. 2–5. The radial coordinate extends up to about 4500 Mpc (some 5.6 patches) and the redshift up to 3.

Figure 2 depicts the function E'/E over these patches, while the functions $M(r)$ and $k(r)$ are presented in Figs. 3 and 4, respectively. Figure 5 depicts the redshift drift for the Szekeres model and compares it with that for the ΛCDM model and for three LTB models: Alnes, Amarzguioui, and Grøn's void model [3] and the so-called constrained García-Bellido–Haugbølle (cGBH) void model [7], both studied in Ref. [39], and Yoo's hump model [54], studied in Ref. [40]. As is well known, the drift for the ΛCDM model is positive up to some redshift [38,39]—this is of course a distinguishing feature for an accelerating FLRW cosmology.

The redshift drift for our Szekeres Swiss-cheese model is negative while for the ΛCDM model it is positive until a redshift 2.5. However, we wish to stress here that the minus sign of the drift appearing in our particular model cannot be considered as a general feature of Szekeres cosmology. This should actually be studied by an analysis extended to a number of other QSS Swiss-cheese models. This will be the subject of future work.

As stressed before, the redshift-drift in our Szekeres model is also compared, in Fig. 5, with that in three LTB
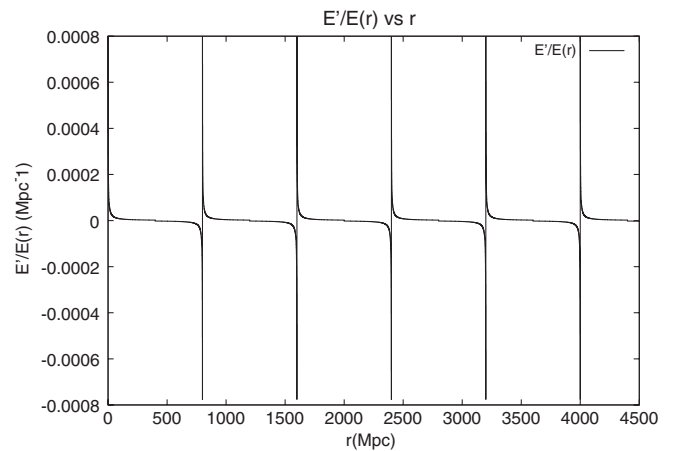
FIG. 2. The $E'/E(r)$ function as a function of the radial coordinate r.
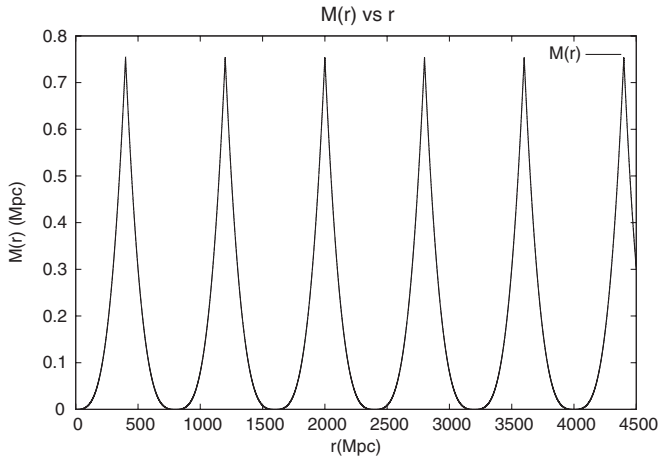
FIG. 3. The effective gravitational mass $M(r)$ as a function of the radial coordinate r.

models: two LTB void models, the Alnes-Amarzguioui-Grøn– type [3] model I and the cGBH model [7] studied in Ref. [39], and a LTB hump model described in Ref. [54] whose redshift drift is shown in Ref. [40]. In the void models, an inner underdensity makes a smooth transition to an outer region with higher density. In the hump model the density profile exhibits a large overdensity near the center. In all three models the observer is centrally located. These models are constructed in order to reproduce to a very good accuracy different cosmological data sets among which are the SNIa data. They show the same general shape for the drift curve as our Szekeres model does, with the drift becoming more negative with increasing z. Note however that the magnitude of the drift in our Szekeres model is higher by a factor of about 2, at a given redshift, in comparison to the LTB models (at those redshifts where the LTB curves show a decline with increasing z). We want also to stress here that, even though the redshift drift of an off-center source observed at the symmetry center of any LTB void model is always negative,
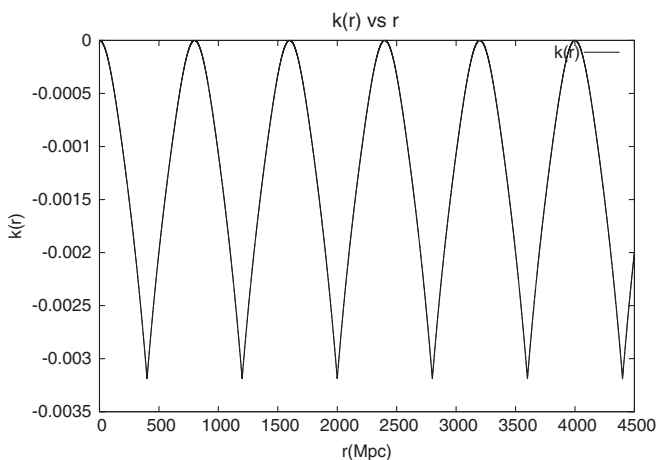
FIG. 4. The $k(r)$ function, determining the model evolution type, as a function of the radial coordinate r.
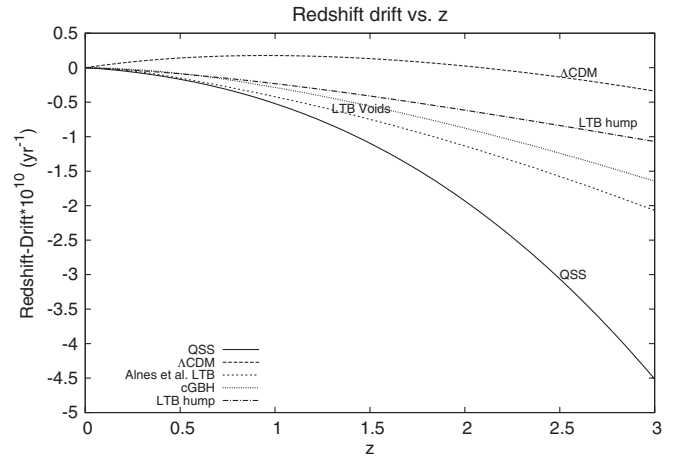
FIG. 5. The redshift drift ($\delta z / \delta t_0$) as a function of the redshift z for the axially symmetric QSS Swiss-cheese model, the ΛCDM model, the cGBH LTB void model [7] (courtesy of Ref. [39]), the Alnes-Amarzguioui-Grøn LTB void model [3] (courtesy: Ref. [39]) and the Yoo LTB hump model [54] (courtesy: Ref. [40]).

this is not obligatorily the case in a LTB hump model [40]. The feature exhibited by the redshift drift in the particular hump model shown in Fig. 5 cannot be therefore generalized to the whole class of such models.

V. FULLY CONSTRAINING THE MODEL DEGREES OF FREEDOM

Inhomogeneous exact models have been sometimes criticized on the ground that they exhibit more degrees of freedom than FLRW models and are thus able to fit more easily the data. In Sec. IV, we have studied a particular axially symmetric QSS Swiss-cheese model able to reproduce the supernova data and we have computed the redshift drift for this model. However, another interesting question to be addressed is: how many and which independent data sets do we need to be able to fully reconstruct an axially symmetric Swiss-cheese QSS model from background observations?

Following Ref. [50], it has been shown in Ref. [51] (Theorem 3.1) that a constant-(x, y) null geodesic exists only in an axially symmetric Szekeres space-time.[1]

One can always find a coordinate system for x and y where, in such a space-time, the functions P and Q obey the set of equations

---

[1]We wish to stress here a misstatement in this Theorem 3.1. It is claimed that there is only one null geodesic with constant x and y in the axially symmetric case. This is not true: the null geodesics that pass through the symmetry axis may have any radial direction and may cross the symmetry axis at different instants of the cosmic time t. So, this is actually a two-parameter family of null geodesics, one parameter defining the azimuthal direction and the other defining the instant of intersection with the axis.

$$(x_0, y_0) = (P, Q) \Rightarrow P' = Q' = 0. \qquad (5.1)$$

Hence, in these coordinates, the model is fully determined, not by six arbitrary functions of r, as in the most general Szekeres model, but only by four. We choose here $M(r)$, $k(r)$, $t_B(r)$ and $S(r)$ or equivalently $E'/E(r)$.

Up to here, we have only at our disposal, to constrain our model, the supernova data used in BC and the redshift drift we have computed in Sec. III to be used for such a purpose in the future. The question is: how many independent data sets do we need to fully constrain the four arbitrary functions of r of such a model assuming these data are measured on the axial null geodesics directed towards the observer?

It has already been shown in Ref. [38] that the combination of luminosity distance and redshift-drift data allows one to fully reconstruct a spherically symmetric spacetime. This applies, in particular, to LTB models. It has also been shown in Ref. [29] that, for any given isotropic observations of the apparent luminosity $l(z)$ and of the galaxy number count $n(z)$, with any given source evolution functions $\hat{L}(z)$ and $\hat{m}(z)$, a set of functions determining a zero-Λ LTB model can be found to make the LTB observational relations fit the observations. We can reword this last statement as follows: the two arbitrary functions of r of a zero-Λ LTB model can be fully determined by two independent sets of observations realized on the observer past light cone.

A natural guess is therefore that an axially symmetric zero-Λ Swiss-cheese Szekeres model needs three independent observation sets to be fully reconstructed. We demonstrate here, using a reasoning inspired from Ref. [29],[2] that this is indeed the case.

Note that, in this section, we work with units in which $c = G = 1$.

A. Coordinate choice

We denote the past null cone issued from the observer at $(t = t_0, r = 0)$ and composed of all the axially directed null geodesics of the Swiss cheese by $t = \hat{t}(r)$. From (2.11), $t = \hat{t}$ satisfies

$$\frac{d\hat{t}}{dr} = -\frac{\Phi'[\hat{t}(r), r] - \Phi[\hat{t}(r), r]E'/E}{\sqrt{1-k}} = -\frac{\hat{\Phi}' - \hat{\Phi}E'/E}{\sqrt{1-k}}, \qquad (5.2)$$

a hat denoting a quantity evaluated on the observer's past light cone.

We now use our freedom to choose the radial coordinate such that, on this past light cone,

---

[2]We wish to correct here an error in Eq. (31) of Ref. [29]. At variance with what is claimed there, the luminosity distance is not the same as the diameter distance but is related to it by the reciprocity theorem [55] expressed by our Eq. (5.17).

$$\frac{\hat{\Phi}' - \hat{\Phi}E'/E}{\sqrt{1-k}} = 1. \qquad (5.3)$$

The equation for the incoming axial null geodesic is then

$$\hat{t}(r) = t_0 - r. \qquad (5.4)$$

With this coordinate choice, (2.7) becomes

$$4\pi\hat{\rho}\hat{\Phi}^2 = \frac{M' - 3ME'/E}{\sqrt{1-k}}, \qquad (5.5)$$

and, on the past light cone, (2.6) must be written, with $\Lambda = 0$,

$$\dot{\hat{\Phi}}^2 = \frac{2M}{\hat{\Phi}} - k. \qquad (5.6)$$

This equation possesses solutions in terms of a parameter $\eta(t, r)$ depending on the sign of k. When written on the past light cone, they become

$$\hat{\Phi} = \frac{M(r)}{K(r)}\hat{\phi}(t, r), \qquad \hat{\xi}(t, r) = \frac{K(r)^{3/2}[\hat{t} - t_B(r)]}{M(r)}. \qquad (5.7)$$

(i) For $k > 0$,

$$K(r) = k, \qquad \hat{\phi} = 1 - \cos\hat{\eta}, \qquad \hat{\xi} = \hat{\eta} - \sin\hat{\eta}. \qquad (5.8)$$

(ii) For $k = 0$,

$$K(r) = 1, \qquad \hat{\phi} = (1/2)\hat{\eta}^2, \qquad \hat{\xi} = (1/6)\hat{\eta}^3. \qquad (5.9)$$

(iii) For $k < 0$,

$$K(r) = -k, \qquad \hat{\phi} = \cosh\hat{\eta} - 1,$$
$$\hat{\xi} = \sinh\hat{\eta} - \hat{\eta}. \qquad (5.10)$$

These expressions tell us the type of evolution for each region, based on the measured data: for $k > 0$, the model expands away from an initial singularity and then recollapses to a final singularity (elliptic evolution); with $k < 0$ the model is either ever-expanding or ever-collapsing, depending on the initial conditions (hyperbolic evolution); $k = 0$ is the intermediate case (parabolic evolution).

B. Differential equations for the arbitrary functions

The total derivative of Φ on the past null cone is

$$\frac{d\hat{\Phi}}{dr} = \hat{\Phi}' + \dot{\hat{\Phi}}\frac{d\hat{t}}{dr}, \qquad (5.11)$$

into which we substitute (5.3) and (5.4) to obtain

$$E'/E = \frac{1}{\hat{\Phi}}\left[\frac{d\hat{\Phi}}{dr} + \hat{\Phi} - \sqrt{1-k}\right]. \qquad (5.12)$$

From (5.6), we have

$$\hat{\Phi} = \pm\sqrt{\frac{2M}{\hat{\Phi}} - k}. \qquad (5.13)$$

Since we are in an expanding Universe, we choose the + sign for $\hat{\Phi}$ in (5.13). Thus, we substitute (5.13) with the + sign into (5.12) and obtain

$$E'/E = \frac{1}{\hat{\Phi}}\left[\frac{d\hat{\Phi}}{dr} + \sqrt{\frac{2M}{\hat{\Phi}} - k} - \sqrt{1-k}\right]. \qquad (5.14)$$

This gives us a first-order differential equation for the arbitrary function $E(r)$ which can be very easily integrated once $\hat{\Phi}$ and the other arbitrary functions $M(r)$ and $k(r)$ are determined.

We wish to write now a first-order differential equation for $M(r)$. We substitute (5.14) into (5.5), which gives

$$\frac{dM}{dr} - \frac{3M}{\hat{\Phi}}\left[\frac{d\hat{\Phi}}{dr} + \sqrt{\frac{2M}{\hat{\Phi}} - k} - \sqrt{1-k}\right]$$
$$= 4\pi\hat{\rho}\hat{\Phi}^2\sqrt{1-k}. \qquad (5.15)$$

Note that, at variance with the differential equation for M obtained in the LTB case in Ref. [29], (5.15) involves not only the observable quantity $\hat{\rho}$ but also the unknown arbitrary function k. This will not invalidate our reasoning but make it a little more complicated.

We aim now at deriving a differential equation for k involving observable quantities, the arbitrary function M, $\hat{\Phi}$ and its total derivatives with respect to r.

The luminosity distance D_L of a source satisfies, on the past light cone of the observer,

$$\hat{D}_L(z) = \sqrt{\frac{\hat{L}(z)}{4\pi\ell(z)}}, \qquad (5.16)$$

with $\hat{L}$ being the absolute luminosity, i.e., the luminosity in the rest frame of the source, and $\ell(z)$ the measured bolometric flux, i.e., integrated over all frequencies, emitted by the source at redshift z.

The area distance D_A, also known as the angular diameter distance, is related to the luminosity distance by the reciprocity theorem [55]:

$$D_A(z) = \frac{D_L(z)}{(1+z)^2}. \qquad (5.17)$$

Therefore, once we obtain a differential equation involving $\hat{D}_A$, it is easy to transform it, through (5.17), into a differential equation involving $\hat{D}_L$, which is a quantity measured on the observer's past light cone, as shown by (5.16).

It has been demonstrated in BC that, for axial geodesics, D_A can be written

$$\frac{d^2 D_A}{ds^2} = -\frac{1}{2}R_{\alpha\beta}k^\alpha k^\beta D_A, \qquad (5.18)$$

where k^α is the null tangent vector, dx^α/ds, and s is the null affine parameter. On an axially directed null geodesic $k^x = k^y = 0$ and (5.18) can thus be written

$$\frac{d^2 D_A}{ds^2} = -\frac{1}{2}[R_{tt}(k^t)^2 + 2R_{tr}k^t k^r + R_{rr}(k^r)^2]D_A. \qquad (5.19)$$

We use

$$\frac{d^2 D_A}{ds^2} = \frac{d^2 D_A}{dr^2}(k^r)^2 + \frac{dD_A}{dr}\frac{dk^r}{ds}. \qquad (5.20)$$

With $E_{,x} = E_{,y} = E_{,rx} = E_{,ry} = 0$ on the axially directed null geodesics, the geodesic equation for r becomes [51]

$$\frac{dk^r}{ds} + 2\frac{\dot{\Phi}_1}{\Phi_1}k^t k^r + \left[\frac{\Phi_1'}{\Phi_1} + \frac{k'}{2(1-k)}\right](k^r)^2 = 0, \qquad (5.21)$$

where

$$\Phi_1 \equiv \Phi' - \Phi E'/E. \qquad (5.22)$$

With our coordinate choice, on the light cone, $k^r = -k^t$. Using (5.21), we insert (5.20) into (5.19) and obtain

$$\frac{d^2\hat{D}_A}{dr^2} + \left[2\frac{(\dot{\hat{\Phi}}_1)}{\hat{\Phi}_1} - \frac{\hat{\Phi}_1' + \hat{\Phi}(E'/E)^2}{\hat{\Phi}_1} - \frac{k'}{2(1-k)}\right]\frac{d\hat{D}_A}{dr}$$
$$+ \frac{1}{2}(\hat{R}_{tt} - 2\hat{R}_{tr} + \hat{R}_{rr})\hat{D}_A = 0. \qquad (5.23)$$

The R_{tr} Ricci tensor component vanishes here, the R_{tt} component is

$$R_{tt} = \frac{3\ddot{\Phi}E'/E - \ddot{\Phi}' - 2\ddot{\Phi}\Phi'/\Phi}{\Phi' - \Phi E'/E}, \qquad (5.24)$$

and the R_{rr} component can be written

$$R_{rr} = \left(\frac{\Phi_1}{1-k}\right)(\ddot{\Phi}' - \ddot{\Phi}E'/E + 2\dot{\Phi}\dot{\Phi}'/\Phi)$$
$$+ \frac{1}{1-k}\left\{2(\dot{\Phi}^2 - 1 + k)(E'/E)^2\right.$$
$$\left. + 2\frac{E'/E}{\Phi}\left[-\Phi'\dot{\Phi}^2 + \Phi'(1-k) - k'\frac{\Phi}{2}\right] + k'\frac{\Phi'}{\Phi}\right\}. \qquad (5.25)$$

Substituting (5.24) and (5.25) written on the light cone into (5.23), we obtain a differential equation involving $\hat{D}_A(r)$, $d\hat{D}_A/dr$ and $d^2\hat{D}_A/dr^2$. However, what the observer measures on her past light cone are not these quantities, but rather $\hat{D}_L(z)$ and its derivatives with respect to the redshift z. We apply therefore

$$\frac{d\hat{D}_A}{dr} = \frac{d\hat{D}_A}{dz}\frac{d\hat{z}}{dr} \qquad (5.26)$$

and

$$\frac{d^2\hat{D}_A}{dr^2} = \frac{d\hat{D}_A}{dz}\frac{d^2\hat{z}}{dr^2} + \frac{d^2\hat{D}_A}{dz^2}\left(\frac{d\hat{z}}{dr}\right)^2, \qquad (5.27)$$

while also using (3.3), written on the light cone as

$$\frac{d\hat{z}}{dr} = (1+\hat{z})\frac{\hat{\Phi}_1}{\sqrt{1-k}}, \qquad (5.28)$$

and the $\hat{D}_L$ expression as given by (5.17). We obtain, after some calculations,

$$\left(\frac{d\hat{D}_L}{dz} - \frac{2\hat{D}_L}{1+\hat{z}}\right)\left\{\hat{\Phi}_1\left[2\frac{\hat{\Phi}_1}{\hat{\Phi}_1} - \frac{\hat{\Phi}_1'}{\hat{\Phi}_1} + \frac{\hat{\Phi}_1}{\sqrt{1-k}} + \frac{1}{1+\hat{z}}\right] + \hat{\Phi}_1'\right\}$$

$$+ \left[(1+\hat{z})\frac{d^2\hat{D}_L}{dz^2} - 4\frac{d\hat{D}_L}{dz} + \frac{6\hat{D}_L}{1+\hat{z}}\right]\frac{(\hat{\Phi}_1)^2}{\sqrt{1-k}}$$

$$+ \frac{\hat{D}_L}{2(1+\hat{z})}\frac{\hat{\Phi}_1}{\sqrt{1-k}}\left[\frac{k'}{\hat{\Phi}} - 2\frac{E'/E}{\hat{\Phi}}(\hat{\Phi}^2 + k - 1) + \hat{\Phi}'\right.$$

$$+ 2\frac{\hat{\Phi}'\hat{\Phi}}{\hat{\Phi}} - \hat{\Phi}E'/E + \frac{1-k}{(\hat{\Phi}_1)^2}\left(3\hat{\Phi}E'/E - 2\frac{\hat{\Phi}'\hat{\Phi}}{\hat{\Phi}} - \hat{\Phi}'\right)\right]$$

$$= 0. \qquad (5.29)$$

To obtain a second-order differential equation for k, we substitute into (5.29) E'/E, as given by (5.14), and $(E'/E)'$ and the partial derivatives of Φ as given in the Appendix. For readability purposes, we leave this task to the interested reader. These are functions of k, k', k'', M, $\hat{\rho}$, $d\hat{\rho}/dz$, $\hat{z}$ and the total derivatives of Φ with respect to r up to second order.

To be able to solve for M and k we need a third differential equation involving $\hat{\Phi}$ and possibly M and k. It is given by (5.28) into which we substitute the expressions for the partial derivatives of $\hat{\Phi}$ as given in the Appendix and that of E'/E as given by (5.14). We obtain

$$\frac{\sqrt{1-k}}{(1+\hat{z})}\frac{d\hat{z}}{dr} = \frac{4M}{\hat{\Phi}^2} + \frac{1}{\sqrt{\frac{2M}{\hat{\Phi}}-k}}\left[\frac{2M}{\hat{\Phi}^2}\frac{d\hat{\Phi}}{dr}\right.$$

$$+ \sqrt{1-k}\left(4\pi\hat{\rho}\,\hat{\Phi} - \frac{3M}{\hat{\Phi}^2}\right) - \frac{k'}{2}\right]$$

$$- \frac{1}{\hat{\Phi}}\sqrt{\frac{2M}{\hat{\Phi}}-k}\left[\frac{d\hat{\Phi}}{dr} + \sqrt{\frac{2M}{\hat{\Phi}}-k} - \sqrt{1-k}\right]. \qquad (5.30)$$

We have thus obtained a set of three differential equations for the unknown functions M, k and $\hat{\Phi}$. However, since the observables, $\hat{\rho}$, $d\hat{\rho}/dz$, $\hat{D}_L$ and derivatives with respect to z and $\hat{z}$ are given in terms of the redshift z, and not of the unobservable coordinate r, we need to write them as functions of r instead of z. This can be performed by using (5.28) and the solution $\hat{z}(r)$ of (5.32) given below in Sec. V C. For readability purposes, we do not write down

here the resulting equation and let the interested reader do the straightforward calculation for herself.

We solve numerically the set of three coupled equations (5.15), (5.29), and (5.30) with the origin conditions $M(r=0) = k(r=0) = \hat{\Phi}(r=0) = 0$ [51] and obtain $M(r)$, $k(r)$ and $\hat{\Phi}(r)$. Then, $E(r)$ proceeds from (5.14).

We have now at our disposal three arbitrary functions, $M(r)$, $k(r)$ and $E(r)$ which are sufficient for fully determining the model with our coordinate choice (5.3). The last integration function $t_B(r)$ proceeds from $M(r)$, $k(r)$ and $\hat{\Phi}$ as follows.

We solve for $\hat{\eta}$ from the first equation in (5.7), (5.8), (5.9), and (5.10). Then t_B follows from

$$\hat{t} - t_B = t_0 - r - t_B = \frac{M}{K^{3/2}}\hat{\xi}. \qquad (5.31)$$

C. Equation for $\hat{z}(r)$

Besides $\hat{\rho}$ and $\hat{D}_L$, another measurable quantity we have at our disposal is the redshift drift as given by (3.12). On the light cone, after replacing the partial derivatives of $\hat{\Phi}$ by their expressions given in the Appendix and using (5.28), this equation can be written

$$\frac{d^2\hat{z}}{dr^2} - \frac{1}{1+\hat{z}}\left(\frac{d\hat{z}}{dr}\right)^2 + \left[(1+\hat{z})\frac{d\hat{z}_0}{dz} - \hat{z}_0\right]\frac{d\hat{z}}{dr} = 0, \qquad (5.32)$$

where $\hat{z}_0(z) = (\delta\hat{z}/\delta t_0)(z)$ is the redshift drift for a given δt_0 as measured by the observer for a source at redshift $\hat{z}$ on her past light cone when she is at $(t_0, r=0)$. This equation gives a second-order differential equation for $\hat{z}$. With the origin condition $\hat{z}(r=0) = 0$ by definition of the redshift, it can be numerically solved from the measurements of $\hat{z}_0$ to yield $\hat{z}(r)$. This allows us to write the $\hat{\Phi}$ total derivatives with respect to z instead of r, by using (5.28).

D. Algorithm

To obtain the functions, M, k, E and t_B from the galaxy number count, $n(z)$, supernova luminosity distance and redshift-drift observations, we propose to proceed as follows:

(1) Take the discrete data $\ell(z, \theta, \phi)$ and $n(z, \theta, \phi)$, and correct them for known observational bias and selection effects. We do not consider here evolution effects. Average them over angles, fit them to some smooth analytic function of z and obtain $\ell(z)$ and $n(z)$.

(2) Assuming a phenomenological $\hat{L}(z)$ law, use (5.16) to obtain $\hat{D}_L(z)$ and then its derivatives up to second order.

(3) Determine from the data a constant average galaxy mass m (we do not consider here galaxy mass evolution) and obtain $\hat{\rho}(z) = mn(z)$.

(4) Assuming observations of the redshift drift have been performed over an elapsed time δt_0 sufficient

to provide a robust data set, $\hat{\hat{z}}_0(z, \theta, \phi)$, average it over all angles, fit it to some smooth analytic function of z and obtain $\hat{\hat{z}}_0(z)$ and its first derivative.

(5) Determine $\hat{z}(r)$ by solving (5.32) and use it to transform the observables $\hat{z}$, $\hat{\rho}$, $d\hat{\rho}/dz$, $\hat{D}_L$ and its derivatives with respect to z into functions of r.

(6) Determine $\hat{\Phi}(r)$, $M(r)$ and $k(r)$ from the set of differential equations (5.30), (5.15), and (5.29).

(7) Knowing $M(r)$, $k(r)$ and $\hat{\Phi}(r)$, determine $E(r)$ by integrating (5.14).

At this stage, we have obtained three arbitrary functions of r which, with our coordinate choice, are enough to fully determine the model. However, for completeness, we give below the recipe to compute the last integration function $t_B(r)$.

(8) Solve for $\hat{\eta}$ from the first equation in (5.7), (5.8), (5.9), and (5.10).

(9) Determine $t_B(r)$ from (5.31).

This is the algorithm that could be applied to an ideal universe, where the redshift is monotonically increasing and where no shell crossing is present to close the past null cone. We make such assumptions here but can be led to a more detailed study of the conditions imposed by them on the data in a future work.

Note that this recipe implies also the existence of a number of particular directions of axial symmetry in the observable Universe. It constitutes another simplifying assumption made at this stage.

To be complete, our above algorithm derivation should include a discussion of the existence and uniqueness of the differential equation set solutions. Given the difficulty of this task, we postpone it to future work and just assume here that solutions actually exist and that some of them, were they to be nonunique, could be selected owing to their physical properties best designed to represent our Universe.

E. Observables pertaining to the studied model

The model studied in Sec. IV has already been shown in BC to be able to reproduce to a good accuracy the supernova data, i.e., the observed luminosity distance-redshift relation. We have also depicted in Fig. 5 the redshift drift for this model. To characterize it completely, we need thus the mass density ρ on the past light cone of the observer at O, as shown in Sec. V. We have therefore computed it as a function of both the radial coordinate r (Fig. 6) and the redshift z (Fig. 7).

Notice that, while ρ/ρ_b possesses a Swiss-cheese-like feature on the spacelike hypersurface $t = t_0$ (Fig. 6), it becomes smoother on the past light cone, while exhibiting anyhow some cusps at the patch borders where the matching conditions are not perfect as already discussed in Sec. IV (Fig. 7). We have been able however to fit it rather accurately to the smooth $(1 + z)^{5.5}$ curve (Fig. 7) with a maximum fractional error of 38% and a mean fractional error of 20%.
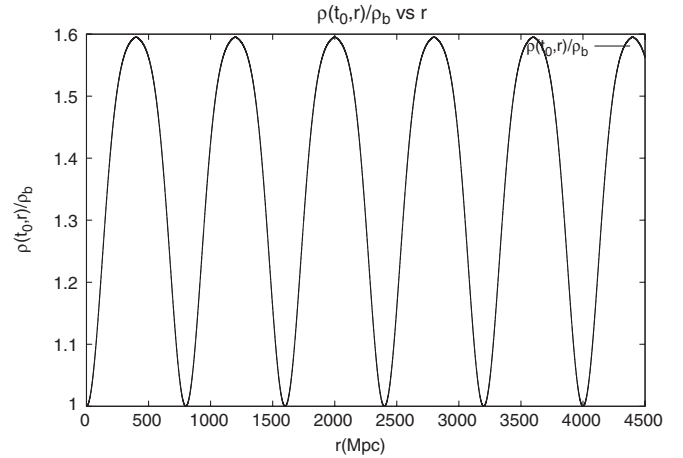
FIG. 6. The ratio of the QSS model mass density $\rho(t_0, r)$ and the background FLRW model mass density ρ_b at the initial instant t_0 on the observer's world line. This quantity can be calculated but cannot be observed since it is in a spacelike relation to the observer.

The redshift drift appears smoother. Here, the nonperfect matching is less visible. While all the model-determining functions are constructed as in a Swiss cheese, Fig. 5 giving the drift on the past light cone from O shows a very smooth curve. We have thus been able to fit it to the smooth $az^b + cz^d$ function with the best fit for $a = -0.023$, $b = 2.46$, $c = -0.029$ and $d = 1.2$ with a maximum fractional error of 12% and a mean fractional error of 2%.

Hence, it is interesting to note that a very patchy underlying inhomogeneous model can correspond to smooth quantities measured on the observer's past light cone. Such a result might be an interesting outcome of algorithms of the kind proposed here, were the Universe such
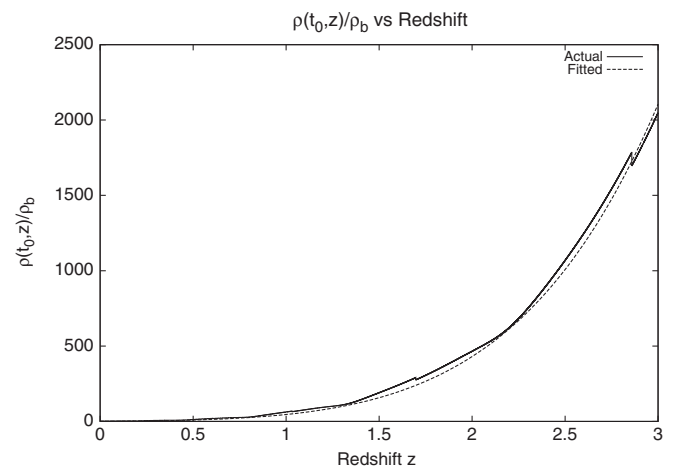
FIG. 7. The ratio of the QSS model mass density $\rho(t_0, z)$ and the background FLRW model mass density ρ_b on the past light cone of the observer at O, before smoothing (solid curve) and after smoothing as described in the text (dotted curve).

that very inhomogeneous solutions able to represent it would correspond to smooth observables.

VI. CONCLUSIONS

The redshift drift was recently proposed in the literature as a way to discriminate between different universe models able to reproduce the current cosmological data without resort to any dark energy component [38–40]. It is considered as an interesting tool for getting rid of the degeneracy which can appear between different solutions. Its expression has been known for a long time in the Friedmannian framework and it was lately calculated for the inhomogeneous spherically symmetric LTB models [40].

We have, in Sec. III, generalized this calculation to the axially symmetric QSS model and given there a new analytic expression for the drift in this model.

Then, we have applied this result to its numerical computation for the axially symmetric QSS Swiss-cheese BC model 5 which was shown in Ref. [25] to be able to reproduce to a good accuracy the supernova data. Comparing it to the ΛCDM drift up to a redshift $z = 3$, we have shown that this effect can be a good discriminator between both models since (i) as it is well known, the drift in the ΛCDM model is positive up to $z = 2.5$, while it is negative with an enhanced decline at high z in our model, and (ii) at redshift $z = 3$, where the drift has become negative for the ΛCDM model, its amplitude is much higher by a factor of ~ 14 in our model.

We have also compared the drift obtained for our model with that displayed in Refs. [39,40] for LTB models. We have found that the redshift drift in our model exhibits the same general shape as in these models but that its magnitude is higher on average by a factor of about 2 at a given redshift. This has been discussed at length in Sec. IV.

However, inhomogeneous exact models have been sometimes criticized on the ground that they exhibit more degrees of freedom than FLRW models and are thus able to fit more easily the data. Therefore, in Sec. V we have addressed the issue of finding how many and which independent data sets we need to be able to fully reconstruct an axially symmetric QSS model from background observations and we have also derived an algorithm for implementing this goal. Of course, we can presume that the choice of the data sets able to constrain the model is not unique, but the observables we have used are the only ones which have allowed us to derive a detailed algorithm for dealing so far with the issue.

Given the rather high amplitude of the drift in our model, some cosmologists might be tempted to use it carelessly as an actual discriminator between QSS Swiss-cheeses and other models. It was indeed studied in Refs. [56–58] how the drift could be measured in the future by the proposed European Extremely Large Telescope instrument CODEX or in Refs. [56,57] by the VLT instrument ESPRESSO. These were claimed in Ref. [39] to be able to discriminate

between ΛCDM and different LTB models in the course of an observation decade. Therefore, since the drift in our model is higher by a factor of 2, some researchers might be led to conclude that a five-year observation period might be sufficient to complete a test for our model. Another possibility to discriminate between inhomogeneous and homogeneous universe models by measuring the redshift drift with the future space-borne gravitational wave interferometer DECIGO/BBO was put forward in Refs. [59,60] where the experiment duration was estimated to be around 5–10 years.

Now, we want to stress that the Swiss-cheese model we studied here is a mere toy model, not designed to be actually put to the test. We are not claiming that our Universe is constructed with axially symmetric patches, nor that we might be located at the origin of one such patch or that the light emitted by distant sources should come to us following axially directed geodesics.

However, we believe that cosmology is a very exciting science which is still in its infancy. For more than 50 years, homogeneous cosmology has been the main subject of study and, despite a number of attractive achievements, it is still facing huge unresolved problems, such as dark matter, dark energy, galaxy formation, etc. Inhomogeneous cosmology is still younger and it needs to progress step by step. This is the reason why, even if after LTB models, Szekeres ones are now coming slowly into play, their tricky properties lead us to begin with the study of the simpler QSS models, hence axial symmetry and its mathematical simplifications.

We are confident that the rather simple algorithm we display here to completely determine an axially symmetric QSS model from background observations will be generalized in the future to the most general QSS model, allowing one therefore to obtain a very interesting representation of our Universe from cosmological data. We are determined to go on working in this direction.

APPENDIX

We give here the expressions of the partial derivatives of $\hat{\Phi}$ needed to perform the calculations in Sec. V.

The first derivative with respect to time is already known from (5.13). We recall it here for completeness:

$$\hat{\Phi} = \sqrt{\frac{2M}{\hat{\Phi}} - k}. \tag{A1}$$

To obtain $\ddot{\Phi}$ on the light cone, we take the derivative of (5.6) with respect to the time coordinate which gives

$$\dot{\hat{\Phi}} = -\frac{M}{\hat{\Phi}^2}. \tag{A2}$$

From (5.11) with our coordinate choice (5.3) and (A1) for $\dot{\hat{\Phi}}$, we get

$$\hat{\Phi}' = \frac{d\hat{\Phi}}{dr} + \dot{\hat{\Phi}}. \tag{A3}$$

To obtain $\dot{\hat{\Phi}}'$, we differentiate (A1) with respect to r and then substitute $\hat{\Phi}'$ as given by (A3) and M' as given by (5.15) into the resulting equation, which gives

$$\dot{\hat{\Phi}}' = \frac{2M}{\hat{\Phi}^2} + \frac{1}{\sqrt{\alpha}}\left[\frac{2M}{\hat{\Phi}^2}\frac{d\hat{\Phi}}{dr} + \sqrt{1-k}\beta - \frac{k'}{2}\right], \tag{A4}$$

where

$$\alpha \equiv \frac{2M}{\hat{\Phi}} - k \tag{A5}$$

and

$$\beta \equiv 4\pi\hat{\rho}\,\hat{\Phi} - \frac{3M}{\hat{\Phi}^2}. \tag{A6}$$

Now, we wish to calculate $\dot{\hat{\Phi}}''$. With our coordinate choice (5.3), we can write

$$\hat{\Phi}' = \sqrt{1-k} + \hat{\Phi}E'/E, \tag{A7}$$

which we differentiate with respect to r to obtain

$$\hat{\Phi}'' = -\frac{k'}{2\sqrt{1-k}} + \hat{\Phi}'E'/E + \hat{\Phi}(E'/E)'. \tag{A8}$$

The expression for $\hat{\Phi}''$ is therefore obtained by substituting into (A8) the expression for $\hat{\Phi}'$ as given by (A3) and those for E'/E as given by (5.14) and for $(E'/E)'$ as calculated below.

Differentiating (5.14) with respect to r and rearranging yields

$$\left(\frac{E'}{E}\right)' = \frac{1}{\hat{\Phi}}\frac{d^2\hat{\Phi}}{dr^2} - \frac{1}{\hat{\Phi}^2}\frac{d\hat{\Phi}}{dr}\left(\frac{d\hat{\Phi}}{dr} + \sqrt{\alpha} - \sqrt{1-k}\right)$$
$$+ \frac{1}{\sqrt{\alpha}}\left[\frac{2M}{\hat{\Phi}^2}\frac{d\hat{\Phi}}{dr} + \beta\sqrt{1-k}\right]$$
$$+ \frac{k'}{2}\left(\frac{1}{\hat{\Phi}\sqrt{1-k}} - \frac{1}{\sqrt{\alpha}}\right) + \frac{3M}{\hat{\Phi}^2}. \tag{A9}$$

After some calculations, we thus obtain for $\hat{\Phi}''$

$$\hat{\Phi}'' = \frac{d^2\hat{\Phi}}{dr^2} + \frac{1}{\hat{\Phi}}\left[3M + \alpha + \sqrt{\alpha}\frac{d\hat{\Phi}}{dr} - \sqrt{\alpha(1-k)}\right]$$
$$+ \frac{1}{\sqrt{\alpha}}\left[\frac{2M}{\hat{\Phi}}\frac{d\hat{\Phi}}{dr} + \sqrt{1-k}\hat{\Phi}\beta - \frac{k'}{2}\hat{\Phi}\right]. \tag{A10}$$

Differentiating (A2) with respect to r and substituting into the resulting equation the expressions for $\hat{\Phi}'$ and M' as given respectively by (A3) and (5.15), we obtain

$$\dot{\hat{\Phi}}' = -\frac{M}{\hat{\Phi}^3}\left(\frac{d\hat{\Phi}}{dr} + \sqrt{\alpha}\right) - \sqrt{1-k}\frac{\beta}{\hat{\Phi}}. \tag{A11}$$

Finally, to obtain $\ddot{\hat{\Phi}}''$, we differentiate $\dot{\hat{\Phi}}'$ with respect to r and obtain

$$\dot{\hat{\Phi}}'' = \frac{2M}{\hat{\Phi}^2\sqrt{\alpha}}\frac{d^2\hat{\Phi}}{dr^2} + \frac{2M}{\hat{\Phi}^3}\left(3\frac{d\hat{\Phi}}{dr} + \sqrt{\alpha}\right) + \sqrt{1-k}\left(12\pi\hat{\rho} - \frac{11M}{\hat{\Phi}^3}\right) - \frac{1}{\alpha^{3/2}}\left[\frac{2M}{\hat{\Phi}^2}\left(\frac{d\hat{\Phi}}{dr} + \sqrt{\alpha}\right) + \sqrt{1-k}\beta - \frac{k'}{2}\right]$$
$$\times\left[\frac{2M}{\hat{\Phi}^2}\frac{d\hat{\Phi}}{dr} + \sqrt{1-k}\beta - \frac{k'}{2}\right] + \frac{1}{\sqrt{\alpha}}\left[\frac{2M}{\hat{\Phi}^3}\left(\frac{d\hat{\Phi}}{dr}\right)^2 + \sqrt{1-k}\left(\frac{3\beta}{\hat{\Phi}}\frac{d\hat{\Phi}}{dr} + 4\pi\hat{\rho}'\hat{\Phi}\right)\right]$$
$$- 3(1-k)\frac{\beta}{\hat{\Phi}} + \frac{2M}{\hat{\Phi}^3}(3M - k) - \frac{k'}{2\sqrt{1-k}}\beta - \frac{k''}{2} + \frac{2M(\hat{\Phi} - 1)}{\alpha\hat{\Phi}^2}\left[\frac{2M}{\hat{\Phi}^2}\frac{d\hat{\Phi}}{dr} + \sqrt{1-k}\beta - \frac{k'}{2}\right], \tag{A12}$$

where we have replaced $\partial/\partial r(d\hat{\Phi}/dr)$ by its expression $\hat{\Phi}'' - \dot{\hat{\Phi}}'$ following from our coordinate choice, with $\hat{\Phi}''$ and $\dot{\hat{\Phi}}'$ as obtained from, respectively, (A10) and (A4) substituted, and where we have also inserted M' as given by (5.15) and $\hat{\Phi}'$ as given by (A3).

We see that this equation includes $\hat{\rho}'$. We use (5.28) and the expressions (A4) of $\dot{\hat{\Phi}}'$, and (A3) of $\hat{\Phi}'$, to write $\hat{\rho}'$ in terms of $d\hat{\rho}/dz$ as

$$\hat{\rho}' = \frac{1+\hat{z}}{\sqrt{1-k}}\left\{\frac{1}{\sqrt{\alpha}}\left[\frac{2M}{\hat{\Phi}^2}\frac{d\hat{\Phi}}{dr} + \sqrt{1-k}\beta - \frac{k'}{2}\right] - \frac{\sqrt{\alpha}}{\hat{\Phi}}\left(\frac{d\hat{\Phi}}{dr} - \sqrt{1-k}\right) + \frac{k}{\hat{\Phi}}\right\}\frac{d\hat{\rho}}{dz}. \tag{A13}$$

Examining the above expressions for $(E'/E)'$ and the different partial derivatives of $\hat{\Phi}$ involved in the set of three coupled differential equations derived in Sec. V, it is easy to conclude that these equations relate $\hat{\Phi}$ and its total derivative with respect to r up to second order, the observables $\hat{\rho}(z)$ and its first derivative with respect to z, $\hat{D}_L$ and its derivatives with respect to z up to second order, and $\hat{z}$, and the arbitrary functions with their derivatives, M, M', k, k', k'', which allows us to solve for $\hat{\Phi}(r)$, $M(r)$ and $k(r)$ with the algorithm described in Sec. V.

[1] M. N. Célérier, Astron. Astrophys. **353**, 63 (2000).
[2] H. Iguchi, T. Nakamura, and K. Nakao, Prog. Theor. Phys. **108**, 809 (2002).
[3] H. Alnes, M. Amarzguioui, and Ø. Grøn, Phys. Rev. D **73**, 083 519 (2006).
[4] D. J. H. Chung and A. E. Romano, Phys. Rev. D **74**, 103 507 (2006).
[5] K. Enqvist and T. Mattsson, J. Cosmol. Astropart. Phys. 02 (2007) 019.
[6] K. Bolejko, PMC Phys. A **2**, 1 (2008); arXiv:astro-ph/0512103.
[7] J. García-Bellido and T. Haugbølle, J. Cosmol. Astropart. Phys. 04 (2008) 003.
[8] J. García-Bellido and T. Haugbølle, J. Cosmol. Astropart. Phys. 09 (2008) 016.
[9] J. P. Zibin, A. Moss, and D. Scott, Phys. Rev. Lett. **101**, 251 303 (2008).
[10] C.-M. Yoo, T. Kai, and K-i Nakao, Prog. Theor. Phys. **120**, 937 (2008).
[11] K. Enqvist, Gen. Relativ. Gravit. **40**, 451 (2008).
[12] S. Alexander, T. Biswas, A. Notari, and D. Vaid, J. Cosmol. Astropart. Phys. 09 (2009) 025.
[13] K. Bolejko and J. S. B. Wyithe, J. Cosmol. Astropart. Phys. 02 (2009) 020.
[14] M. N. Célérier, K. Bolejko, and A. Krasiński, Astron. Astrophys. **518**, A21 (2010).
[15] T. Biswas, A. Notari, and W. Valkenburg, J. Cosmol. Astropart. Phys. 11 (2010) 030.
[16] A. Moss, J. P. Zibin, and D. Scott, Phys. Rev. D **83**, 103 515 (2011).
[17] S. Nadathur and S. Sarkar, Phys. Rev. D **83**, 063 506 (2011).
[18] T. Kai, H. Kozaki, K. Nakao, Y. Nambu, and C. Yoo, Prog. Theor. Phys. **117**, 229 (2007).
[19] V. Marra, E. W. Kolb, S. Matarrese, and A. Riotto, Phys. Rev. D **76**, 123 004 (2007).
[20] N. Brouzakis, N. Tetradis, and E. Tzavara, J. Cosmol. Astropart. Phys. 02 (2007) 013.
[21] V. Marra, E. W. Kolb, and S. Matarrese, Phys. Rev. D **77**, 023 003 (2008).
[22] N. Brouzakis, N. Tetradis, and E. Tzavara, J. Cosmol. Astropart. Phys. 04 (2008) 008.
[23] N. Brouzakis and N. Tetradis, Phys. Lett. B **665**, 344 (2008).
[24] T. Biswas and A. Notari, J. Cosmol. Astropart. Phys. 06 (2008) 021.
[25] K. Bolejko and M.-N. Célérier, Phys. Rev. D **82**, 103 510 (2010).
[26] K. Bolejko and R. Sussman, Phys. Lett. B **697**, 265 (2011).
[27] W. Stoeger, G. F. R. Ellis, and S. Nel, Classical Quantum Gravity **9**, 509 (1992).
[28] R. Maartens, N. P. Humphreys, D. R. Matravers, and W. R. Stoeger, Classical Quantum Gravity **13**, 253 (1996); **13**, 1689(E) (1996).
[29] N. Mustapha, C. Hellaby, and G. F. R. Ellis, Mon. Not. R. Astron. Soc. **292**, 817 (1997).

[30] M. E. Araújo and W. R. Stoeger, Phys. Rev. D **60**, 104 020 (1999).
[31] M. Zumalacárregui, J. García-Bellido, and P. Ruiz-Lapuente, arXiv:1201.2790.
[32] J. P. Zibin and A. Moss, Classical Quantum Gravity **28**, 164005 (2011).
[33] P. Bull, T. Clifton, and P. G. Ferreira, Phys. Rev. D **85**, 024 002 (2012).
[34] T. Clifton, P. G. Ferreira, and K. Land, Phys. Rev. Lett. **101**, 131 302 (2008).
[35] A. E. Romano, arXiv:1105.1864.
[36] A. Sandage, Astrophys. J. **136**, 319 (1962).
[37] G. McVittie, Astrophys. J. **136**, 334 (1962).
[38] J.-P. Uzan, C. Clarkson, and G. F. R. Ellis, Phys. Rev. Lett. **100**, 191 303 (2008).
[39] M. Quartin and L. Amendola, Phys. Rev. D **81**, 043 522 (2010).
[40] C. M. Yoo, T. Kai, and K-i Nakao, Phys. Rev. D **83**, 043 527 (2011).
[41] M.-N. Célérier, Astron. Astrophys. **543**, A71 (2012).
[42] J. P. Zibin, Phys. Rev. D **84**, 123508 (2011).
[43] R. K. Sheth and R. van de Weygaert, Mon. Not. R. Astron. Soc. **350**, 517 (2004).
[44] P. Szekeres, Commun. Math. Phys. **41**, 55 (1975).
[45] A. Krasiński and K. Bolejko, Phys. Rev. D **83**, 083 503 (2011).
[46] A. Krasiński, Phys. Rev. D **84**, 023 510 (2011).
[47] V. A. Ruban, Pis'ma Red. Zh. Eksp. Teor. Fiz. **8**, 669 (1968) [Sov. Phys. JETP Lett. **8**, 414 (1968)]; Reprinted, with historical comments: Gen. Relativ. Gravit. **33**, 363 (2001).
[48] V. A. Ruban, Zh. Eksp. Teor. Fiz. **56**, 1914 (1969) [Sov. Phys. JETP **29**, 1027 (1969)]; reprinted, with historical comments: Gen. Relativ. Gravit. **33**, 375 (2001).
[49] C. Hellaby, Classical Quantum Gravity **13**, 2537 (1996).
[50] B. C. Nolan and U. Debnath, Phys. Rev. D **76**, 104 046 (2007).
[51] K. Bolejko, A. Krasiński, C. Hellaby, and M.-N. Célérier, *Structures in the Universe by Exact Methods—Formation, Evolution, Interactions* (Cambridge University Press, Cambridge, England, 2010).
[52] J. Plebański and A. Krasiński, *An Introduction to General Relativity and Cosmology* (Cambridge University Press, Cambridge, England, 2006).
[53] K. Bolejko, Gen. Relativ. Gravit. **41**, 1737 (2009).
[54] C.-M. Yoo, Prog. Theor. Phys. **124**, 645 (2010).
[55] I. M. H. Etherington, Philos. Mag. **15**, 761 (1933).
[56] S. Cristiani *et al.*, Nuovo Cimento Soc. Ital. Fis. B **122**, 1165 (2007).
[57] V. D'Odorico (CODEX/EXPRESSO team), arXiv:0708.1258.
[58] J. Liske *et al.*, Mon. Not. R. Astron. Soc. **386**, 1192 (2008).
[59] K. Yagi, A. Nishizawa, and C.-M. Yoo, arXiv:1112.6040.
[60] K. Yagi, A. Nishizawa, and C.-M. Yoo, arXiv:1204.1670.